Intense circularly polarized attosecond pulse generation from relativistic laser plasmas using few-cycle laser pulses

Guangjin Ma,[1,*] **Wei Yu,**[1] **M. Y. Yu,**[2,3] **Baifei Shen**[1] **and Laszlo Veisz**[4,5]

[1]*State Key Laboratory of High Field Laser Physics, Shanghai Institute of Optics and Fine Mechanics, Chinese Academy of Sciences, Shanghai 201800, China*
[2]*Institute of Fusion Theory and Simulation, Zhejiang University, Hangzhou 310027, China*
[3]*Institute for Theoretical Physics I, Ruhr University, Bochum, D-44780 Germany*
[4]*Max-Planck-Institut für Quantenoptik, D-85748 Garching, Germany*
[5]*Department of Physics, Umeå University, SE-901 87 Umeå, Sweden*

[*]*guangjin@siom.ac.cn*

Abstract: We have investigated the polarization of attosecond light pulses generated from relativistic few-cycle laser pulse interaction with the surface of overdense plasmas using particle-in-cell simulation. Under suitable conditions, a desired polarization state of the generated attosecond pulse can be achieved by controlling the polarization of the incident laser. In particular, an elliptically polarized laser pulse of suitable ellipticity can generate an almost circularly polarized attosecond pulse without compromising the harmonic generation efficiency. The process is thus applicable as a new tabletop circularly-polarized XUV radiation source for probing attosecond phenomena with high temporal resolution.

OCIS codes: (320.7110) Ultrafast nonlinear optics; (190.4160) Multiharmonic generation; (260.5430) Polarization; (350.5400) Plasmas.

References and links

1. S.-Y. Xu, M. Neupane, C. Liu, D. Zhang, A. Richardella, L. A. Wray, N. Alidoust, M. Leandersson, T. Balasubramanian, J. Sánchez-Barriga, O. Rader, G. Landolt, B. Slomski, J. H. Dil, J. Osterwalder, T.-R. Chang, H.-T. Jeng, H. Lin, A. Bansil, N. Samarth, and M. Z. Hasan, "Hedgehog spin texture and berrys phase tuning in a magnetic topological insulator," Nature Phys. **8**, 616–622 (2012).
2. I. Gierz, M. Lindroos, H. Höchst, C. R. Ast, and K. Kern, "Graphene sublattice symmetry and isospin determined by circular dichroism in angle-resolved photoemission spectroscopy," Nano Lett. **12**, 3900–3904 (2012).
3. G. Schütz, M. Knülle, and H. Ebert, "Magnetic circular x-ray dichroism and its relation to local moments," Phys. Scripta **1993**, 302 (1993).
4. T. Fan, P. Grychtol, R. Knut, C. Hernández-García, D. D. Hickstein, D. Zusin, C. Gentry, F. J. Dollar, C. A. Mancuso, C. W. Hogle, O. Kfir, D. Legut, K. Carva, J. L. Ellis, K. M. Dorney, C. Chen, O. G. Shpyrko, E. E. Fullerton, O. Cohen, P. M. Oppeneer, D. B. Miloševi, A. Becker, A. A. Jaroń-Becker, T. Popmintchev, M. M. Murnane, and H. C. Kapteyn, "Bright circularly polarized soft x-ray high harmonics for x-ray magnetic circular dichroism," Proc. Natl. Acad. Sci. USA **112**, 14206–14211 (2015).
5. Y. Liu, G. Bian, T. Miller, and T.-C. Chiang, "Visualizing electronic chirality and berry phases in graphene systems using photoemission with circularly polarized light," Phys. Rev. Lett. **107**, 166803 (2011).
6. J. Schmidt, A. Guggenmos, M. Hofstetter, S. H. Chew, and U. Kleineberg, "Generation of circularly polarized high harmonic radiation using a transmission multilayer quarter waveplate," Opt. Express **23**, 33564–33578 (2015).
7. S. Long, W. Becker, and J. K. McIver, "Model calculations of polarization-dependent two-color high-harmonic generation," Phys. Rev. A **52**, 2262–2278 (1995).

#262655 Received 5 Apr 2016; revised 21 Apr 2016; accepted 23 Apr 2016; published 28 Apr 2016

8. O. Kfir, P. Grychtol, E. Turgut, R. Knut, D. Zusin, D. Popmintchev, T. Popmintchev, H. Nembach, J. M. Shaw, A. Fleischer, H. Kapteyn, M. Murnane, and O. Cohen, "Generation of bright phase-matched circularly-polarized extreme ultraviolet high harmonics," Nature Photon. **9**, 99 (2015).
9. D. D. Hickstein, F. J. Dollar, P. Grychtol, J. L. Ellis, R. Knut, C. Hernández-García, D. Zusin, C. Gentry, J. M. Shaw, T. Fan, K. M. Dorney, A. Becker, A. Jaroń-Becker, H. C. Kapteyn, M. M. Murnane, and C. G. Durfee, "Non-collinear generation of angularly isolated circularly polarized high harmonics," Nature Photon. **9**, 743 (2015).
10. U. Teubner and P. Gibbon, "High-order harmonics from laser-irradiated plasma surfaces," Rev. Mod. Phys. **81**, 445–479 (2009).
11. S. Kahaly, S. Monchocé, H. Vincenti, T. Dzelzainis, B. Dromey, M. Zepf, P. Martin, and F. Quéré, "Direct observation of density-gradient effects in harmonic generation from plasma mirrors," Phys. Rev. Lett. **110**, 175001 (2013).
12. B. Dromey, D. Adams, R. Hörlein, Y. Nomura, S. G. Rykovanov, D. C. Carroll, P. S. Foster, S. Kar, K. Markey, P. McKenna, D. Neely, M. Geissler, G. D. Tsakiris, and M. Zepf, "Diffraction-limited performance and focusing of high harmonics from relativistic plasmas," Nature Phys. **5**, 146–152 (2009).
13. B. Dromey, S. Kar, C. Bellei, D. C. Carroll, R. J. Clarke, J. S. Green, S. Kneip, K. Markey, S. R. Nagel, P. T. Simpson, L. Willingale, P. McKenna, D. Neely, Z. Najmudin, K. Krushelnick, P. A. Norreys, and M. Zepf, "Bright multi-kev harmonic generation from relativistically oscillating plasma surfaces," Phys. Rev. Lett. **99**, 085001 (2007).
14. Y. Nomura, R. Hörlein, P. Tzallas, B. Dromey, S. Rykovanov, Z. Major, J. Osterhoff, S. Karsch, L. Veisz, M. Zepf, D. Charalambidis, F. Krausz, and G. D. Tsakiris, "Attosecond phase locking of harmonics emitted from laser-produced plasmas," Nature Phys. **5**, 124–128 (2009).
15. B. Dromey, S. Rykovanov, M. Yeung, R. Hörlein, D. Jung, D. C. Gautier, T. Dzelzainis, D. Kiefer, S. Palaniyppan, R. Shah, J. Schreiber, H. Ruhl, J. C. Fernandez, C. L. S. Lewis, M. Zepf, and B. M. Hegelich, "Coherent synchrotron emission from electron nanobunches formed in relativistic laser-plasma interactions," Nature Phys. **8**, 804–808 (2012).
16. A. Debayle, J. Sanz, and L. Gremillet, "Self-consistent theory of high-order harmonic generation by relativistic plasma mirror," Phys. Rev. E **92**, 053108 (2015).
17. R. Lichters, J. Meyer-ter-Vehn, and A. Pukhov, "Short-pulse laser harmonics from oscillating plasma surfaces driven at relativistic intensity," Phys. Plasmas **3**, 3425–3437 (1996).
18. T. Baeva, S. Gordienko, and A. Pukhov, "Theory of high-order harmonic generation in relativistic laser interaction with overdense plasma," Phys. Rev. E **74**, 046404 (2006).
19. D. an der Brügge and A. Pukhov, "Enhanced relativistic harmonics by electron nanobunching," Phys. Plasmas **17**, 033110 (2010).
20. S. G. Rykovanov, M. Geissler, J. Meyer-ter-Vehn, and G. D. Tsakiris, "Intense single attosecond pulses from surface harmonics using the polarization gating technique," New J. Phys. **10**, 025025 (2008).
21. T. Baeva, S. Gordienko, and A. Pukhov, "Relativistic plasma control for single attosecond x-ray burst generation," Phys. Rev. E **74**, 065401 (2006).
22. K. Gál and S. Varró, "Polarization properties of high harmonics generated on solid surfaces," Opt. Commun. **198**, 419 – 431 (2001).
23. G. Veres, J. S. Bakos, I. B. Földes, K. Gál, Z. Juhász, G. Kocsis, and S. Szatmári, "Polarization of harmonics generated by ultrashort krf-laser pulses on solid surfaces," EPL **48**, 390 (1999).
24. P. Gibbon, "Harmonic generation by femtosecond laser-solid interaction: A coherent "water-window" light source?" Phys. Rev. Lett. **76**, 50–53 (1996).
25. L. A. Gizzi, D. Giulietti, A. Giulietti, P. Audebert, S. Bastiani, J. P. Geindre, and A. Mysyrowicz, "Simultaneous measurements of hard x rays and second-harmonic emission in fs laser-target interactions," Phys. Rev. Lett. **76**, 2278–2281 (1996).
26. M. Yeung, B. Dromey, S. Cousens, T. Dzelzainis, D. Kiefer, J. Schreiber, J. H. Bin, W. Ma, C. Kreuzer, J. Meyer-ter-Vehn, M. J. V. Streeter, P. S. Foster, S. Rykovanov, and M. Zepf, "Dependence of laser-driven coherent synchrotron emission efficiency on pulse ellipticity and implications for polarization gating," Phys. Rev. Lett. **112**, 123902 (2014).
27. P. Heissler, R. Hörlein, M. Stafe, J. Mikhailova, Y. Nomura, D. Herrmann, R. Tautz, S. Rykovanov, I. Földes, K. Varjú, F. Tavella, A. Marcinkevicius, F. Krausz, L. Veisz, and G. D. Tsakiris, "Toward single attosecond pulses using harmonic emission from solid-density plasmas," Appl. Phys. B **101**, 511–521 (2010).
28. E. Rácz, I. Földes, G. Kocsis, G. Veres, K. Eidmann, and S. Szatmári, "On the effect of surface rippling on the generation of harmonics in laser plasmas," Appl. Phys. B **82**, 13–18 (2006).
29. F. Krausz and M. Ivanov, "Attosecond physics," Rev. Mod. Phys. **81**, 163–234 (2009).
30. G. Ma, W. Dallari, A. Borot, F. Krausz, W. Yu, G. D. Tsakiris, and L. Veisz, "Intense isolated attosecond pulse generation from relativistic laser plasmas using few-cycle laser pulses," Phys. Plasmas **22**, 033105 (2015).
31. L. Veisz, D. Rivas, G. Marcus, X. Gu, D. Cardenas, J. Mikhailova, A. Buck, T. Wittmann, C. M. S. Sears, S.-W. Chou, J. Xu, G. Ma, D. Herrmann, O. Razskazovskaya, V. Pervak, and F. Krausz, "Generation and applications of sub-5-fs multi- 10-TW light pulses," in *2013 Conference on Lasers and Electro-Optics Pacific Rim,* (Optical

#262655 Received 5 Apr 2016; revised 21 Apr 2016; accepted 23 Apr 2016; published 28 Apr 2016

Society of America, 2013), paper TuD2_3.
32. H. Xu, W. Chang, H. Zhuo, L. Cao, and Z. Yue, "Parallel programming of 2(1/2)-dimensional pic under distributed-memory parallel environments," Chin. J. Comput. Phys. **19**, 305 (2002).
33. N. M. Naumova, J. A. Nees, I. V. Sokolov, B. Hou, and G. A. Mourou, "Relativistic generation of isolated attosecond pulses in a λ^3 focal volume," Phys. Rev. Lett. **92**, 063902 (2004).
34. M. Born and E. Wolf, *Principles of Optics: Electromagnetic Theory of Propagation, Interference and Diffraction of Light* (Cambridge University, 1999).
35. A. P. Tarasevitch, R. Kohn, and D. von der Linde, "Towards intense attosecond pulses: using two beams for high order harmonic generation from solid targets," J. Phys. B: At. Mol. Opt. Phys. **42**, 134006 (2009).

1. Introduction

Circularly polarized light in the extreme ultra violet (XUV) and soft x-ray regions has proven to be very useful for applications including the direct measurement of quantum phases in graphene and topological insulators [1, 2], the XUV magnetic circular dichroism spectroscopy [3, 4], as well as the reconstruction of band structure and modal phases in solids [5]. Currently, such radiation is mainly available at large scale synchrotron sources and the time resolution is much larger than the sub-laser cycle time scale, limiting its wide availability and time resolving power. Although novel XUV optics can be used to convert XUV polarization [6], it is often subject to limited bandwidth and low transmission efficiency. It has great significance to realize a table-top circularly polarized attosecond XUV source directly by using the laser.

Polarization-dependent two-color high-harmonic generation (HHG) has been considered more than two decades ago [7], and very recently production of bright circularly polarized XUV light by HHG in noble gases has been realized experimentally [8, 9]. In fact, the field has become a focus of research in the nonlinear optics of HHG. Compared to HHG from noble gases, HHG from plasma surfaces [10–28] does not subject to the limitation of maximum applied laser intensity and can thus use the state-of-the-art terawatt and petawatt laser technology, which will improve attosecond pulse energy, making it potentially useful to pump-probe experiments [29]. There is a strong motivation to seek circularly polarized attosecond XUV light source by HHG from plasma surfaces.

Many authors have considered harmonic intensity and polarization state [17,20–28] for HHG from plasma surfaces; however, the ellipticity of harmonics was rarely discussed. Attosecond pulse with circular polarization requires two orthogonally polarized harmonic components correlated with each other. This correlation expresses in terms of the same spectral intensity and half π spectral phase difference independent of frequency in its spectral range. The situation for HHG from plasma surfaces is similar to HHG from noble gases; a circularly polarized laser pulse is generally not suitable to generate circularly polarized laser harmonics. Under normal incidence geometry, it is not efficient in driving the motion of electron population at plasma surfaces which is required to Doppler upshift the laser fundamental frequency [17–19]. Under oblique incidence, although a circularly polarized incident laser has equal energy in its $p-$ and $s-$polarized components, the harmonic yields from these two polarization components are not the same. In order to efficiently generate a circularly polarized attosecond light pulse, it seems that oblique incidence is preferred; and it is required to fine tune the polarization state of an elliptically polarized laser pulse in relative intensity and phase between its two orthogonally polarized components.

In this paper we investigate the polarization of attosecond light pulses generated from relativistic few-cycle laser pulse interaction with the surface of overdense plasmas. Firstly, the carrier-envelope phase φ_{CEP} of the laser is tuned to within the range $0.7\pi \lesssim \varphi_{\mathrm{CEP}} \lesssim 1.8\pi$ and plasma scale length L to within $0.3\lambda_{\mathrm{L}} \lesssim L \lesssim 0.7\lambda_{\mathrm{L}}$ for generating intense isolated attosecond pulse with $p-$polarization [30]. The polarization of the incident laser pulse is then fine tuned to a regime where both the spectral intensity and spectral phase relations between the two or-

#262655 Received 5 Apr 2016; revised 21 Apr 2016; accepted 23 Apr 2016; published 28 Apr 2016

thogonally polarized harmonic components satisfy the requirements for a circularly polarized attosecond light pulse. The main goal of this work is to proposing a new way to generate attosecond pulse with circular polarization or at least with elliptical polarization and a high degree of ellipticity. The laser parameters used in this paper, including among others the 5 fs FWHM pulse duration, are approximately realized using LWS-20 laser system [31].

2. Attosecond pulse properties in a typical interaction scenario

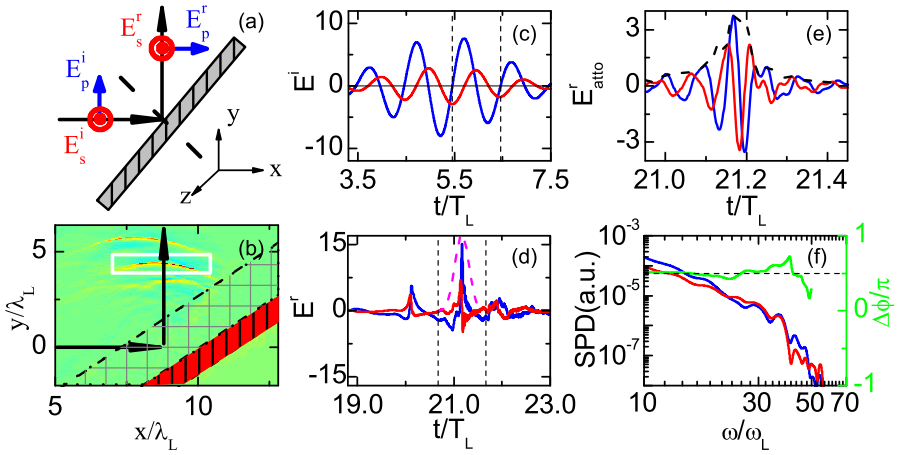

Fig. 1. (a) Laser pulse obliquely incident onto a plane plasma target. Incident $p-$ and $s-$polarized electric field (E_p^i and E_s^i) are in y and z directions; reflected $p-$ and $s-$polarized electric field (E_p^r and E_s^r) are in x and z directions. (b) Reflected $p-$polarized electric field $E_p^r(x,y)$. Areas filled with red color and with grid pattern correspond to constant density and exponential density layers. (c) Incident electric field components E_p^i and E_s^i. (d) Reflected electric field components E_p^r and E_s^r. (e) Filtered electric field components and the total magnitude $[(E_{p,\mathrm{atto}}^r)^2+(E_{s,\mathrm{atto}}^r)^2]^{1/2}$, black dashed line. (f) SPDs for the two field components of the strongest burst and the phase difference between them, green solid line. In (c) to (f), blue and red solid curves are respectively for the $p-$ and $s-$polarized light. Magenta dashed line in (d) is a one-cycle long unit Chebyshev window used to select the strongest burst; its real amplitude is 1. The white rectangle in (b) as well as the two black dashed lines in (c) and (d) mark the cycle for the strongest attosecond pulse emission. Laser and plasma parameters are $E_\mathrm{L}=10$, $\theta=20^\circ$, $\varphi_\mathrm{CEP}=1.17\pi$, $w_0=1.6\lambda_\mathrm{L}$, $\tau_\mathrm{L}=1.875T_\mathrm{L}$ and $L=0.43\lambda_\mathrm{L}$.

As in Fig. 1(a), we consider a laser pulse incident obliquely onto a plane plasma layer at incidence angle $\alpha=45^\circ$. The plasma layer has initially only one dimensional density distribution along its surface normal. The simulation is performed using the 2D PIC code LAPINE [32]. The incident laser pulse propagates along x-axis and has Gaussian spatial and temporal profiles with the normalized electric field at focus given by $\mathbf{E}^i(t)=E_\mathrm{L}\exp(-y^2/w_0^2)\exp[-2\ln 2(t/\tau_\mathrm{L})^2]\{\hat{\mathbf{y}}\cos(2\pi t+\varphi_\mathrm{CEP})\cos\theta+\hat{\mathbf{z}}\cos(2\pi t+\varphi_\mathrm{CEP}+\pi/2)\sin\theta\}$. E_L is the peak laser field normalized by $mc\omega_\mathrm{L}/e$; w_0 is the $1/e$ waist size normalized to laser wavelength λ_L; m, ω_L and e, the electron rest mass, laser fundamental frequency and electron charge respectively. τ_L is the intensity full-width-half-maximum (FWHM) laser pulse duration normalized to laser period T_L. Throughout this paper we assume $E_\mathrm{L}=10$, which corresponds to a laser intensity of 2×10^{20} W/cm^2 for a laser central wavelength λ_L of 800 nm; $\tau_\mathrm{L}=1.875T_\mathrm{L}$, which corresponds to a FWHM duration of 5 fs. The density profile of the interacting plasma

#262655 Received 5 Apr 2016; revised 21 Apr 2016; accepted 23 Apr 2016; published 28 Apr 2016

has an exponential interface layer in the front with scale length of L. It rises from $0.2n_c$ up to a maximum of $90n_c$ and then it is followed by a $1\lambda_L$ thick constant density distribution, where n_e and n_i are electron and ion fluid densities normalized by critical density n_c at ω_L. The simulation is performed for moving ions with charge number $Z = 10$ and ion to electron mass ratio $m_i/m = 50000$. The resolution used is $\Delta x = \Delta y = 2.5 \times 10^{-3}\lambda_L$ and $\Delta t = 1.6 \times 10^{-3}T_L$.

The incident laser pulse is focused at the critical density inside the plasma layer. Its waist size is $w_0 = 1.6\lambda_L$, corresponding to a FWHM diameter of 1.5 μm, making the interaction near to the λ^3 regime [33]. However, as shown in Fig. 1(b), the reflected beam is still well-collimated around the specular reflection direction. This probably because we used a much higher target density compared to that in [33]. The incident laser pulse is recorded at $x = y = 0$, as shown in Fig. 1(b). It is elliptically polarized with ellipticity of $\sigma = \tan\theta = 0.36$ ($\theta = 20^\circ$). The reflected field is recorded at $y = 6.4\lambda_L$ and at an x coordinate where the reflected light energy fluence is at the maximum, as is shown in Fig. 1(d). Both components of the reflected electric field are strongly modulated. They are naturally attosecond spikes even without filtering. These spikes occur at the same time in the p and s components; each pair constitutes the components of a single burst. After filtering with a spectral band containing the 10th to 30th laser harmonics (H10-H30), the strongest burst results in a single isolated attosecond pulse and all other weaker ones result in side pulses having negligible intensity. Field components of the filtered attosecond pulse $E^r_{p,\mathrm{atto}}$ and $E^r_{s,\mathrm{atto}}$ as well as its field magnitude $[(E^r_{p,\mathrm{atto}})^2 + (E^r_{s,\mathrm{atto}})^2]^{1/2}$ are shown in Fig. 1(e). Their corresponding spectral power densities (SPDs) as well as their spectral phase difference $\Delta\phi$ are shown in Fig. 1(f). Note that, to emphasize our interested physics, we have gated the reflected field from the emission cycle with a one-cycle long Chebyshev window before the Fourier analysis. This is to smooth the curves in Fig. 1(f) by precluding the interference due to the weak side pulses. Field magnitude curve in Fig. 1(e) (black dashed curve) is almost smooth with very shallow modulations. The SPD curves of the two polarization components in Fig. 1(f) are similar in shape and more or less overlapped. The spectral phase difference between them is flat with a value of around $\pi/2$. All these features are in agreement with a high degree of ellipticity for the attosecond pulse $\sigma_{\mathrm{atto}} = 0.79$, which is obtained by evaluating the Stokes parameters [34]. The flat and $\pi/2$ spectral phase difference is understandable by checking the structures of the selected cycle from the reflected electric field in Fig. 1(d). A unipolar peak for p polarization implies phase locked "cosine" waves; while a bipolar peak for s polarization implies phase locked "sine" waves. These two categories of waves have phase difference of $\pi/2$ between each other.

3. Attosecond pulse polarization control

To illustrate the idea of attosecond pulse polarization control, we have performed a systematic study through simulation using the 1D PIC code LPIC++ [17]. In 1D simulation, the effect of finite focal spot size is not simulated. We consider two cases: 1) Incident laser pulse is linearly polarized with the normalized electric filed given by $\mathbf{E}^i(t) = E_L \exp[-2\ln 2(t/\tau_L)^2]\cos(2\pi t + \varphi_{\mathrm{CEP}})(\hat{\mathbf{e}}_p \cos\theta + \hat{\mathbf{e}}_s \sin\theta)$. 2) Incident laser pulse is elliptically polarized with the normalized electric field given by $\mathbf{E}^i(t) = E_L \exp[-2\ln 2(t/\tau_L)^2][\hat{\mathbf{e}}_p \cos(2\pi t + \varphi_{\mathrm{CEP}})\cos\theta + \hat{\mathbf{e}}_s \cos(2\pi t + \varphi_{\mathrm{CEP}} + \pi/2)\sin\theta]$. For these two cases, the polarization of the laser pulse is varied continuously through the parameter θ, while all other parameters are kept the same as in the 2D simulation of the previous section. In an actual experiment where the optical pulse output from the laser system is linearly polarized, a half-wave plate is inserted for the first case, while an additional quarter-wave plate is inserted after this half-wave plate for the second case. The variation of the parameter θ is realized by rotation of the half wave plate in each case.

The left and right columns of Fig. 2 show polarization control through linearly and elliptically polarized laser pulses respectively. Every energy efficiency in the figure is defined as

#262655 Received 5 Apr 2016; revised 21 Apr 2016; accepted 23 Apr 2016; published 28 Apr 2016

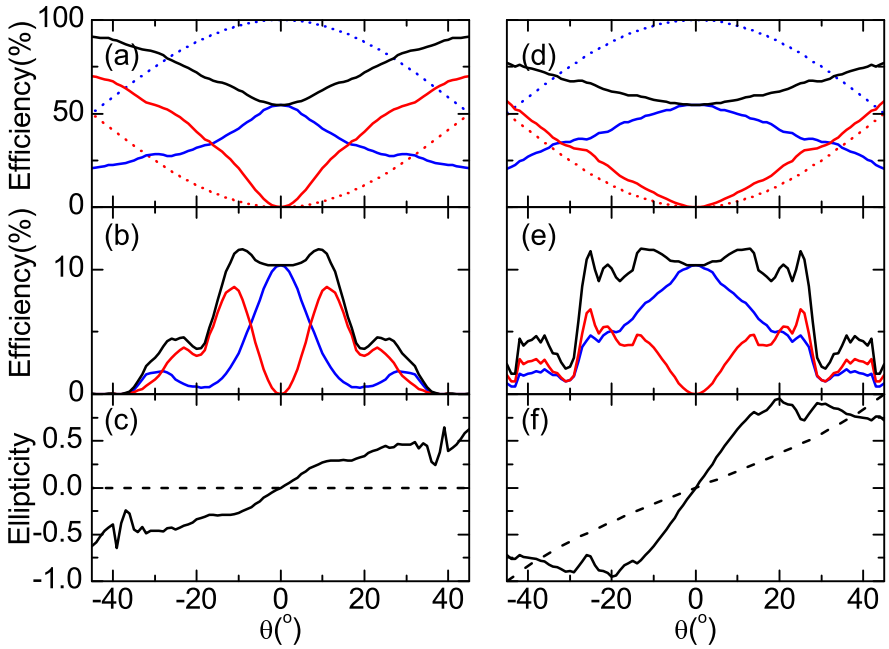

Fig. 2. Polarization control with linearly polarized laser (left column) and with elliptically polarized laser (right column). θ dependence of (a) and (d) the efficiency of the $p-$polarized, $s-$polarized as well as the overall reflected light from the whole spectral range (blue, red and black solid). The energy proportion of the $p-$ and $s-$polarized light in the incident laser pulse (blue and red dashed). (b) and (e) the $p-$polarized, $s-$polarized as well as the overall energy efficiency of the selected attosecond pulse from harmonics H10-H50 (blue, red and black solid). (c) and (f) the ellipticity of the selected attosecond pulse synthesized from H10-H50 (black solid) and of the incident laser pulse (black dashed). The scan resolution for θ is 1°. Laser and plasma parameters are $E_L = 10$, $\varphi_{CEP} = 1.17\pi$, $\tau_L = 1.875T_L$ and $L = 0.43\lambda_L$.

the ratio of the corresponding energy to the energy of the incident laser pulse. When $\theta = 0$, laser pulse is purely $p-$polarized. The energy efficiency for the reflected light from the whole spectral range is only 55%, with the rest energy mainly absorbed by plasma electrons. The selected (strongest) attosecond pulse from the 10th to 50th laser harmonics (H10-H50) is linearly polarized ($\sigma_{atto} = 0$) and its energy efficiency is as high as 10%. As in Fig. 2(a) and 2(d), when laser pulse polarization is rotated off from the p polarization direction, the energy efficiency decreases for $p-$polarized, increases for $s-$polarized as well as the overall reflected light. The energy efficiency for $p-$polarized reflected light is always smaller than the corresponding energy proportion in the incident laser pulse, showing a net absorption of $p-$polarized light by plasma electrons. While the energy efficiency for $s-$polarized reflected light is always larger than the corresponding energy proportion in the incident laser pulse, showing a net emission of $s-$polarized light from plasma electrons. In other words, the reflected s polarization component is using energy from the p polarization component in the incident laser pulse [35]. This explains that, for a range of $|\theta|$ in Fig. 2(b) and 2(e), the attosecond pulse energy efficiency from $s-$polarized harmonics is comparable or even higher than that from $p-$polarized harmonics; although the s polarization component has lower energy than the p polarization component in the incident laser pulse. For linearly polarized laser pulse, as in Fig. 2(b), the overall energy efficiency for the selected attosecond pulse in the $|\theta| > 45^\circ$ regime is orders of magnitude lower

#262655 Received 5 Apr 2016; revised 21 Apr 2016; accepted 23 Apr 2016; published 28 Apr 2016

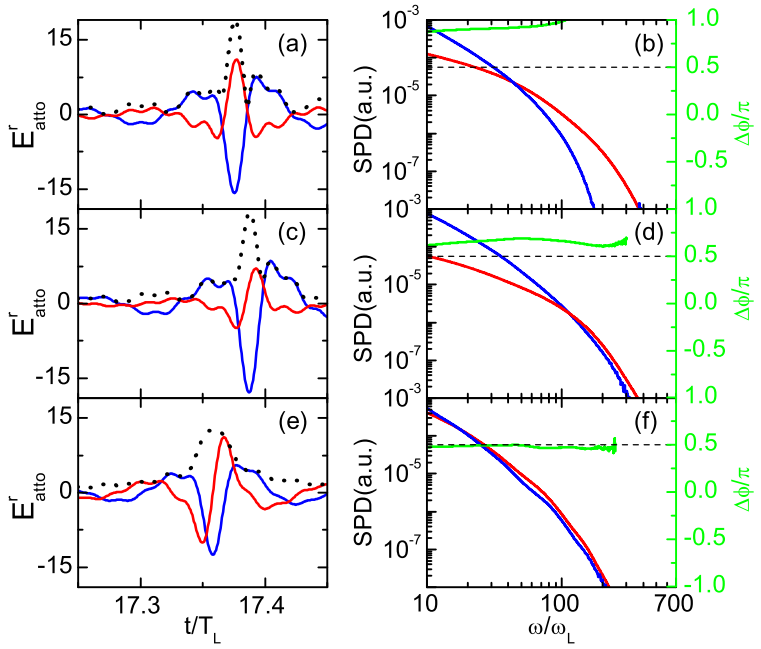

Fig. 3. Temporal (left column) and spectral (right column) features of the selected attosecond pulse. (a), (c) and (e) $p-$polarized $E^r_{p,\mathrm{atto}}$ (blue solid), $s-$polarized $E^r_{s,\mathrm{atto}}$ (red solid) electric field, and the electric field magnitude $[(E^r_{p,\mathrm{atto}})^2+(E^r_{s,\mathrm{atto}})^2]^{1/2}$ (black dashed) of the selected attosecond pulse. (b), (d) and (f) Blue and red solid, the $p-$ and $s-$polarized SPDs. Green solid curve, spectral phase difference between the two polarization components. (a) and (b) $\theta = 5^\circ$. (c) and (d) $\theta = 5^\circ$ ($\sigma = 0.09$). (e) and (f) $\theta = 20^\circ$ ($\sigma = 0.36$). Incident laser pulse for (a) and (b) is linearly polarized. Incident laser pulses for (c) and (d), (e) and (f) are elliptically polarized. Other laser and plasma parameters are the same as in Fig. 2.

than that for $\theta = 0$ case and thus not of interest. There exists an optimum $|\theta| \approx 10^\circ$ where the attosecond pulse overall energy efficiency is at maximum. Although the incident laser pulse is linearly polarized, the generated attosecond pulse generally shows a certain degree of ellipticity. However, it still approaches linear polarization for small $|\theta|$s, as in Fig. 2(c). For elliptically polarized laser, as in Fig. 2(e), there exists a $|\theta|$ range ($|\theta| \lesssim 25^\circ$) where the overall energy efficiency for the selected attosecond pulse almost does not change. In this regime, as $|\theta|$ ($|\sigma| = |\tan\theta|$) increases, the generated attosecond pulse changes from linear polarization to almost circular polarization $|\sigma_{\mathrm{atto}}| \approx 0.95$ at $|\theta| \approx 20^\circ$ ($|\sigma| \approx 0.36$). It is important to mention that the selected attosecond pulse has overall energy efficiency comparable to the regime where the incident laser pulse is purely $p-$polarized ($\theta = 0$).

To show the effect of laser polarization on the temporal and spectral features of the generated attosecond pulse, we choose one instance $\theta = 5^\circ$ using linearly polarized laser pulse as shown in Fig. 3(a) and 3(b); and two instances $\theta = 5^\circ$ and $\theta = 20^\circ$ using elliptically polarized laser pulse as shown in Fig. 3(c) and 3(d), Fig. 3(e) and 3(f). When laser pulse is linearly polarized with small $\theta = 5^\circ$, the two electric field components of the generated attosecond pulse are different in amplitudes and nearly π out of phase (in antiphase) as shown in Fig. 3(a). Their SPD curves are quite different in shape. Their spectral phase difference $\Delta\phi$ is almost flat with value around π as shown in Fig. 3(b). In other words, the generated attosecond pulse approaches

#262655 Received 5 Apr 2016; revised 21 Apr 2016; accepted 23 Apr 2016; published 28 Apr 2016

linear polarization. These features are in agreement with a small ellipticity value $\sigma_{\text{atto}} \approx 0.14$ through evaluating the Stokes parameters. When laser pulse is elliptically polarized with small $\theta = 5^\circ$ ($\sigma = 0.09$), the two electric field components of the generated attosecond pulse are very different in amplitudes and near $\pi/2$ out of phase as shown in Fig. 3(c). Their SPD curves are also quite different in shape with spectral phase difference $\Delta\phi$ slightly larger than $\pi/2$ as shown in Fig. 3(d). The generated attosecond pulse is elliptically polarized with an ellipticity of $\sigma_{\text{atto}} \approx 0.32$. When laser pulse is elliptically polarized with $\theta = 20^\circ$ ($\sigma = 0.36$), the two electric field components of the generated attosecond pulse are almost the same in amplitudes and around $\pi/2$ out of phase as shown in Fig. 3(e). Their SPD curves are almost the same in shape in the whole spectral range. The spectral phase difference between the two components $\Delta\phi$ is very flat and close to $\pi/2$ as shown in Fig. 3(f). The generated attosecond pulse is almost circularly polarized with ellipticity as high as $\sigma_{\text{atto}} \approx 0.95$. Note that $\Delta\phi \approx \pi$ in Fig. 3(b), while $\Delta\phi \approx \pi/2$ in Fig. 3(d) and 3(f); this phase difference is very probably determined by that of the incident laser pulse. We also checked other instances. When the incident laser pulse is linearly polarized, we are not able to match both the spectral intensity and the spectral phase difference $\Delta\phi$ to that required for a circularly polarized attosecond light pulse. When the incident laser pulse is elliptically polarized, however, for all instances where $20^\circ < |\theta| < 45^\circ$, both the spectral shapes and the spectral phase difference $\Delta\phi$ approximately satisfy these two requirements. These are in agreement with the high ellipticity values $|\sigma_{\text{atto}}|$ in the range shown in Fig. 2(f). But, for larger $|\theta|s$, the degree of ellipticity drops and the attosecond pulse energy efficiency is not as high as the $|\theta| \approx 20^\circ$ regime.

For the above interaction conditions, it is possible to generate a circularly polarized attosecond light pulse simply by adjusting the parameter θ of the elliptically polarized incident laser pulse. We have also tried different spectral ranges other than H10-H50, and have got results from which we could draw the same conclusion. However, at other interaction conditions, adjustment of θ might not be enough. For example, when laser and plasma parameters are located in the range $0.2\pi \lesssim \varphi_{\text{CEP}} \lesssim 1.3\pi$ and $0.13\lambda_{\text{L}} \lesssim L \lesssim 0.26\lambda_{\text{L}}$ [30], it was not possible to generate an attosecond pulse with ellipticity $|\sigma_{\text{atto}}|$ higher than 0.7. In this case, adjustment of an additional "knob" is possible. This "knob" is the phase difference between the p and s polarization components of the incident laser pulse which was previously set to be $\pi/2$ using a quarter-wave plate. Tuning of this phase difference is possible using the phase change difference between the $p-$ and $s-$polarized light from reflective surface at different incidence angles [34]. For the mentioned case, we have succeeded to increase the ellipticity of the generated attosecond pulse to higher values through this method after the tuning using θ.

4. Discussions and conclusions

To conclude, the polarization properties of attosecond light pulses generated from the surface of overdense plasmas are investigated. Based on the results, we propose that, if the laser and plasma parameters are controlled [30], through the manipulation of the incident laser pulse polarization, an intense circularly polarized attosecond light pulse from plasma surfaces can be generated which benefits many interesting applications. This attosecond pulse has energy conversion efficiency comparable to its purely $p-$polarized correspondent. A 2D PIC simulation is performed to show the feasibility of the control scheme when the incident laser pulse is tightly focused.

Acknowledgments

The work was supported by the National Natural Science Foundation of China (11304331, 11174303, 11374262), the National Basic Research Program of China (2013CBA01504), the Fundamental Research Funds for Central Universities, the Munich Center for Advanced Pho-

tonics (MAP), DFG Project Transregio TR18, as well as the Euratom research and training programme 2014-2018 under grant agreement No. 633053 within the framework of the EUROfusion Consortium.

#262655 Received 5 Apr 2016; revised 21 Apr 2016; accepted 23 Apr 2016; published 28 Apr 2016